A&A 638, A3 (2020)
https://doi.org/10.1051/0004-6361/201937183
© L. Margulès et al. 2020

Astronomy & Astrophysics

Millimeter wave spectroscopy of cyanoketene (NC–CH=C=O) and an observational search in the ISM*

L. Margulès[1], B. A. McGuire[2], R. A. Motiyenko[1], C. Brogan[2], T. Hunter[2], A. Remijan[2], and J. C. Guillemin[3]

[1] Laboratoire de Physique des Lasers, Atomes, et Molécules, UMR CNRS 8523, Université de Lille I, 59655 Villeneuve d'Ascq Cédex, France
e-mail: laurent.margules@univ-lille.fr
[2] National Radio Astronomy Observatory, Charlottesville, VA 22903, USA
[3] Univ Rennes, Ecole Nationale Supérieure de Chimie de Rennes, CNRS, ISCR UMR6226, 35000 Rennes, France

Received 24 November 2019 / Accepted 3 March 2020

ABSTRACT

Context. Ketene was detected in the interstellar medium (ISM) in 1977. Until now, only one derivative, the ketenyl radical, has been observed in this medium. Due to its large dipole moment value, cynaoketene is one of the best candidates for possible ketene derivative detection.
Aims. To date, the measurements of the rotational spectra have been limited to 60 GHz. The extrapolation of the prediction in the millimeter wave domain is inaccurate and does not permit an unambiguous detection.
Methods. The rotational spectra were re-investigated up to 330 GHz. Using the new prediction cyanoketene was sought after in a variety of astronomical sources: NGS 63341, SgrB2(N), and ASAI sources.
Results. A total of 1594 transitions were newly assigned and fitted together with those from previous studies, reaching quantum numbers up to $J = 82$ and $K_a = 24$. Watson's asymmetric top Hamiltonian in the I^r representation was used for the analysis; both reductions A and S were tested. Logically, the S reduction gave the best results confirming that the molecule is very close to the prolate limit. Cynaoketene was not found in ISM; upper limits to the column density were derived in each source.

Key words. ISM: molecules – methods: laboratory: molecular – submillimeter: ISM – molecular data – line: identification

1. Introduction

Ketene (ethenone, $H_2C{=}C{=}O$) was detected in the interstellar medium (ISM) more than 43 years ago (Turner 1977), and the only derivative, the ketenyl radical (HC=C=O), was observed 38 years later (Agúndez et al. 2015). In contrast, formaldehyde, a compound containing one less carbon and discovered 8 years before ketene (Snyder et al. 1969), has many derivatives detected in the ISM such as acetaldehyde, propanal, propenal, propynal, cyanoformaldehyde, methyl and ethyl formate, formamide, and acetamide[1] (McGuire 2018). However, it should be noted that many derivatives of ketene are very reactive compounds and have never been synthesized. Consequently, the microwave and millimetric spectra of simple substituted ketenes, such as hydroxy-, amino-, formate-, or ethynylketene, are missing. Ketene and methylketene, a simple substituted derivative, are easily isolated on a preparative scale by flash vacuum thermolysis of the corresponding carboxylic anhydride but are unstable compounds in the condensed phase at a temperature higher than −80°C. Only very recently has the millimetric spectrum of methylketene been reported (Bermúdez et al. 2018) but this compound has not yet been detected. It is therefore too early to conclude that there are no substituted ketenes in the ISM before searching for several derivatives in this medium. Cyanides represent a ubiquitous group of large astronomical molecules in the ISM, and are some of the most abundant and easily detectable in a wide range of environments. Simple cyanides, such as HCN, are found in nearly all astronomical environments ranging from comets to external galaxies. The cyanoketene, 3-oxo-2-propenenitrile (NCCH=C=O), a six-atom molecule containing only one hydrogen atom, appears to be a good candidate for the ISM. Using lab conditions to reproduce the chemistry on the interstellar grains, cyanoketene was found in the photolysis of cyanoacetylene with an oxygen atom generated from ozone, the photolysis of water with cyanoacetylene (Guennoun et al. 2005) or dicyanoacetylene (Guennoun et al. 2004). Cyanoketene is more thermodynamically stable than isomers such as cyanoethynol (NC–C≡C–OH), cyanooxirene (NC(c-C=CH-O), or 3-imino-1,2-propadien-1-one (HN=C=C=C=O) (Maier et al. 1998). Combined with its physical properties and the presence of potential precursors in the ISM push us to record and analyze its millimetric spectrum. Using these species as both physical and chemical diagnostics can provide a better understanding and calibration of the physical environments where these species are found and of the formation of large astronomical molecules in general.

2. Experimental design

The flash vacuum thermolysis of 2-cyanoacetyl chloride at 750°C produced cyanoketene with one equivalent of hydrogen chloride (Bock et al. 1981). The gaseous flow leaving the oven was directly introduced into the cell of the spectrometer.

* Global fit, fitting files, and prediction catalog are only available at the CDS via anonymous ftp to cdsarc.u-strasbg.fr (130.79.128.5) or via http://cdsarc.u-strasbg.fr/viz-bin/cat/J/A+A/638/A3
[1] http://www.astrochymist.org/astrochymist_ism.html

Open Access article, published by EDP Sciences, under the terms of the Creative Commons Attribution License (https://creativecommons.org/licenses/by/4.0), which permits unrestricted use, distribution, and reproduction in any medium, provided the original work is properly cited.

Measurements in the frequency range under investigation (150–330 GHz) were performed using the Lille spectrometer (Zakharenko et al. 2015). The absorption cell was a stainless-steel tube (6 cm in diameter, 220 cm in length). The sample pressure and temperature during measurements were about 10 Pa and room temperature, and the line width was limited by Doppler broadening. The frequency range 150–330 GHz was covered with various active and passive frequency multipliers from VDI Inc. and an Agilent synthesizer (12.5–18.25 GHz) was used as the source of radiation. Estimated uncertainties for measured line frequencies are 30 kHz and 50 kHz depending on the observed S/N and the frequency range.

3. Analysis of the spectra

The first paper on the rotational spectra of cyanoketene was published by Hahn et al. (2004). The spectra of the parent molecule were measured in the centimeter-wave domain up to 60 GHz. These latter authors also measured the spectra of five isotopic species and calculated the structure of the molecule. The planarity of the molecule was confirmed and the nuclear quadrupole coupling of ^{14}N was also measured. Using Stark spectroscopy, Hahn et al. (2004) was able to determine accurate values of the dipole moment (μ_a 2.844 D and $\mu_b = 2.112$ D), finding that it is usually large due to a CN group. This causes dense and intense rotational spectra in the millimeter and submillimeter wave range.

The analysis was relatively straightforward starting from predictions based on Hahn et al. (2004) parameters. First the most intense transitions, the ^aR ones, were analyzed and fitted up to 330 GHz. They were shifted by only a few megahertz from initial predictions. Subsequently, ^bR and ^bQ lines were sought and included in the fit up to 330 GHz. We used ASFIT (Kisiel 2001) for the fitting, and predictions were made with SPCAT (Pickett 1991). The global fits included the 70 microwave transitions from Hahn et al. (2004), and 1594 from this work. The maximal quantum numbers are $J = 82$ and $K_a = 24$. We first attempted to use a Waston's A-reduced Hamiltonian for the analysis, however this reduction was unable to robustly treat K_a values greater than 18. This is perhaps because the molecule is quite close to the prolate limit case ($\kappa = 0.982$), and thus would be better treated by a Waston's S-reduced Hamiltonian. The root mean square for A and S reduction considering the full dataset is respectively 210.5 and 24.5 kHz, using 26 parameters for A reduction and 23 for S reduction. Here we only provide the fitting results using the reduction S. In order to compare our parameters with the ones from Hahn et al. (2004), we refitted these data using reduction S. Results can be found in Table 1. Some of the new measurements are in Table 2. Figure 1 shows an example of an observed spectrum. Higher numbers of lines in the experimental spectrum compared to the predicted one come from excited vibrational states.

The complete version of the global fit Table (S1) is supplied at the CDS. The fitting files useable with SPFIT, namely .lin (S2), .par (S3), which contain the measured lines and the spectroscopic parameters respectively, and the prediction .cat (S4) are also available at the CDS.

4. Radioastronomical observations

4.1. Sources

We conducted a search for cyanoketene in a variety of astronomical sources. The observational details of these datasets have all been presented elsewhere (see Table 3); only a brief description is provided here. Because these are nondetections, source-specific and molecule-specific parameters (e.g., source size, excitation temperature) must be assumed in order to calculate an upper limit. In each case, we used parameters representative of each source and complex molecules in that source from the literature references provided in the respective tables.

NGC 6334I. NGC 6334I is a nearby (~1.3 kpc; Chibueze et al. 2014) high-mass star-forming region. The data toward

Table 1. Spectroscopic parameters of cyanoketene in MHz – Reduction S.

Parameter	This work [a]	Hahn et al. (2004) [b]
A	29601.17783 (98) [c]	29601.2097 (76)
B	2812.14944 (11)	2812.15030 (88)
C	2563.72222 (11)	2563.72331 (77)
$D_J \times 10^3$	1.539026 (76)	1.5385 (32)
$D_{JK} \times 10^3$	−115.00801 (47)	−114.967 (97)
$D_K \times 10^3$	2813.778 (55)	2814.1 (13)
$d_1 \times 10^3$	−0.3688395 (72)	−0.36860 (15)
$d_2 \times 10^3$	−0.0091383 (12)	−0.009248 (32)
$H_J \times 10^6$	0.006213 (22)	0.00957 (27)
$H_{JK} \times 10^6$	−0.21768 (16)	
$H_{KJ} \times 10^6$	−24.0191 (27)	−27.8 (11)
$H_K \times 10^6$	807.50 (86)	891. (37)
$h_1 \times 10^9$	2.3535 (20)	2.360 (23)
$h_2 \times 10^9$	0.13074 (31)	0.311 (12)
$h_3 \times 10^9$	0.04377 (17)	
$L_J \times 10^{12}$	−0.0.0382 (22)	
$L_{JJK} \times 10^{12}$	1.555 (17)	
$L_{JK} \times 10^9$	−0.05033 (14)	
$L_{KKJ} \times 10^9$	10.0790 (97)	
$l_1 \times 10^{12}$	−0.01585 (18)	
$l_3 \times 10^{15}$	−1.170 (38)	
$l_4 \times 10^{15}$	−0.0579 (72)	
$P_{KKJ} \times 10^{12}$	−3.206 (10)	
Number of distinct lines	1664	70
Standard deviation of the fit (in kHz)	24.5	39.4
Weighted deviation of fit	0.75	

Notes. [a]Watson's S reduction has been used in the representation I^r. [b]Data from Hahn et al. (2004) originally treated with A reduction but fitted here in the S reduction. [c]Numbers in parentheses are one standard deviation in units of the least significant figures.

Table 2. Measured frequencies of cyanoketene and residuals from the fit.

Upper level			Lower level			Frequency (Unc.)	o.-c.
J''	K''_a	K''_c	J'	K'_a	K'_c	(in MHz)	(in MHz)
50	0	50	49	0	49	258564.279 (0.030)	0.0158
51	0	51	50	0	50	263664.044 (0.030)	0.0072
52	0	52	51	0	51	268763.111 (0.030)	−0.0033
53	0	53	52	0	52	273861.449 (0.030)	0.0080
54	0	54	53	0	53	278958.964 (0.030)	−0.0029
56	0	56	55	0	55	289151.434 (0.030)	−0.0021
57	0	57	56	0	56	294246.325 (0.030)	0.0276
58	0	58	57	0	57	299340.182 (0.030)	−0.0115
59	0	59	58	0	58	304433.094 (0.030)	0.0037
60	0	60	59	0	59	309524.912 (0.030)	−0.0438
61	0	61	60	0	60	314615.773 (0.030)	0.0131
62	0	62	61	0	61	319705.459 (0.030)	−0.0154
63	0	63	62	0	62	324794.050 (0.030)	−0.0224
64	0	64	63	0	63	329881.526 (0.030)	−0.0024

Notes. Full fit is available at the CDS: S1.

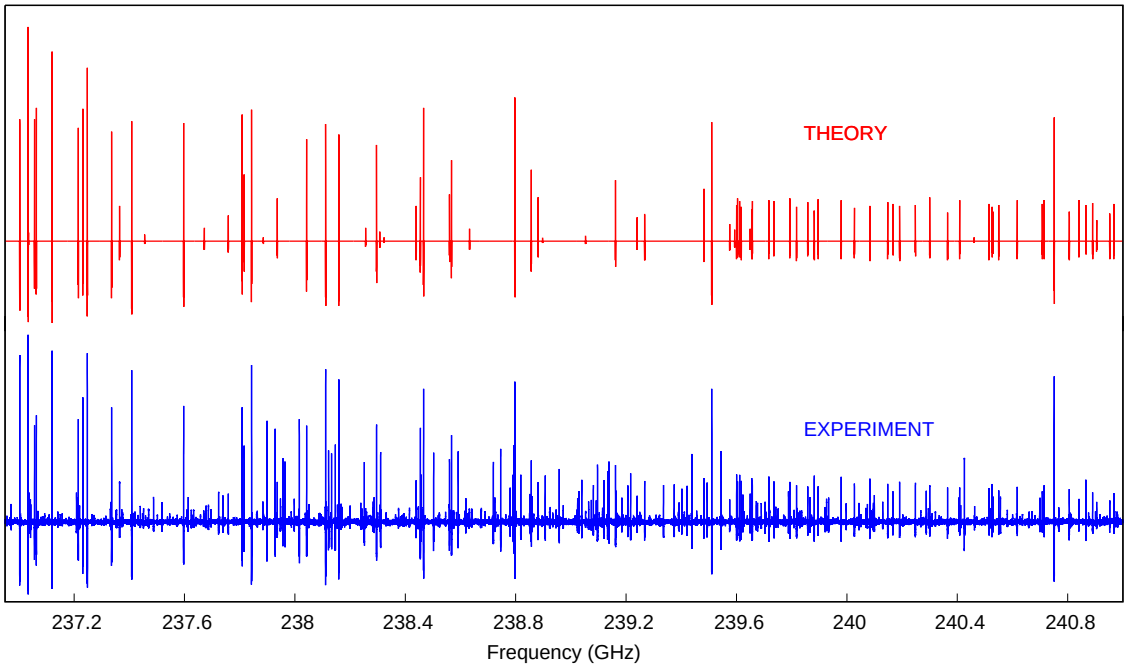

Fig. 1. Predicted (in red) and observed (in blue) rotational spectrum of NC–CH=C=O between 236.9 and 241.3 GHz. The low-frequency region of the spectrum shown here is dominated by a series of R-type transitions, $J = 44$–43, while the high-frequency region is dominated by a series of Q-type transitions, $K_a = 5$–4. The slight inconsistency between predicted and observed spectrum intensities is due to source power and detector sensitivity variations.

Table 3. Source parameters assumed for cyanoketene in each of the sets of observations.

Source	Telescope	θ_s [(a)] ($''$)	T_{bg} (K)	ΔV (km s^{-1})	T_b [(†)] (mK)	T_{ex} (K)	Refs.
NGC 6334I	ALMA	–	28.2	3.2	10.0 [(b)]	135	1
Sgr B2(N)	GBT	20	19.2	25.0	3.7	5	2, 14, 15
Sgr B2(N)	IRAM	2.2	5.2	5.0	10.9	120	3
Barnard 1	IRAM	–	2.7	0.8	2.5	10	4, 5
IRAS 4A	IRAM	–	2.7	5.0	2.3	21	4, 6
L1157B1	IRAM	–	2.7	8.0	1.4	60	7
L1157mm	IRAM	–	2.7	3.0	2.8	60	7
L1448R2	IRAM	–	2.7	8.0	2.4	60	8
L1527	IRAM	–	2.7	0.5	1.9	12	8, 9
L1544	IRAM	–	2.7	0.5	2.3	10	10, 11
SVS13A	IRAM	0.3	2.7	3.0	7.5	80	4, 6
TMC1	IRAM	–	2.7	0.3	6.5	7	12, 13

Notes. [(a)]Except where noted, the source is assumed to fill the beam. [(b)]For these interferometric observations, the intensity is given in mJy beam^{-1} rather than mK. [(†)]Taken either as the 1σ rms noise level at the location of the target line, or for line confusion limited spectra, the reported rms noise of the observations.
References. [1] McGuire et al. (2018a); [2] Neill et al. (2012); [3] Belloche et al. (2013); [4] Melosso et al. (2018); [5] Cernicharo et al. (2018); [6] Higuchi et al. (2018); [7] McGuire et al. (2015); [8] Jørgensen et al. (2002); [9] Araki et al. (2017); [10] Hily-Blant et al. (2018); [11] Crapsi et al. (2005); [12] McGuire et al. (2018b); [13] Gratier et al. (2016); [14] Remijan et al. (2008); [15] McGuire et al. (2016).

NGC 6334I are from ALMA projects #2015.A.00022.T and #2017.1.00717.S, and were extracted from coordinates (J2000) $\alpha = 17{:}20{:}53.374$, $\delta = -35{:}46{:}58.34$. The dataset was imaged at a uniform angular resolution of $0''.26 \times 0''.26$ (McGuire et al. 2017).

Table 4. Harmonic vibrational frequencies of cyanoketene determined at the wB97XD/6-311++G(d,p) level of theory and basis set.

Mode	Frequency (cm^{-1})
1	147.0412
2	396.4186
3	426.5524
4	534.6230
5	607.2004
6	668.5193
7	987.6967
8	1138.4369
9	1417.8312
10	2284.9982
11	2380.7996
12	3223.3903

Sgr B2(N). At a distance of ~8.3 kpc (Reid et al. 2014), Sgr B2(N) is perhaps the most bountiful target for new detections of organic molecules (McGuire 2018). Molecules in this source are typically seen either in emission from warm, compact cores or cold, extended cores and in absorption against a nonthermal background continuum (McGuire et al. 2016; Hollis et al. 2007; Belloche et al. 2013). We used two publicly available datasets to cover both possible scenarios. The Prebiotic Interstellar Molecular Survey (PRIMOS) observations of the region cover the range from 1 to 50 GHz, and are most sensitive to cold, extended populations (Neill et al. 2012), whereas the IRAM 30 m survey of the region near 3 mm provides sensitivity to the warm, compact components (Belloche et al. 2013).

ASAI sources. The remaining sources are from the publicly available Astrochemical Surveys at IRAM (ASAI) Large

Table 5. Upper limits to cyanoketene and the line parameters used to calculate them in each of the sets of observations.

Source	Frequency (MHz)	Transition ($J'_{K_a,K_c} - J''_{K_a,K_c}$)	E_u (K)	$S_{ij}\mu^2$ (bye^2)	Q (Q_{rot}, Q_{vib}) [a]	N_T (cm^{-2})	$N(H_2)$ (cm^{-2})	X_{H_2}	Refs. $N(H_2)$
NGC 6334I	[*]294595.9	$26_{6,20} - 26_{5,21}$	137.0	58.2	23610 (18112, 1.30)	$\leq 6.6 \times 10^{15}$	–	–	–
Sgr B2(N) [b]	26251.4	$5_{1,5} - 4_{1,4}$	5.1	38.1	129 (129, 1.00)	$\leq 3.6 \times 10^{12}$	1×10^{24}	$\leq 4 \times 10^{-12}$	1
Sgr B2(N) [c]	[*]102317.1	$19_{3,17} - 18_{3,16}$	60.7	146.9	18642 (15178, 1.23)	$\leq 2.4 \times 10^{15}$	1×10^{24}	$\leq 2 \times 10^{-9}$	1
Barnard 1	101463.0	$4_{2,3} - 3_{1,2}$	7.7	8.4	365 (365, 1.00)	$\leq 3.1 \times 10^{11}$	1.5×10^{23}	$\leq 2 \times 10^{-12}$	3
IRAS 4A	88954.8	$17_{1,17} - 16_{1,16}$	39.8	134.3	1111 (1111, 1.00)	$\leq 1.2 \times 10^{12}$	3.7×10^{23}	$\leq 4 \times 10^{-12}$	3
L1157B1	[*]91519.7	$17_{5,13} - 16_{5,12}$	71.7	123.1	5529 (5366, 1.03)	$\leq 8.9 \times 10^{11}$	1×10^{21}	$\leq 9 \times 10^{-10}$	3
L1157mm	[*]102294.4	$19_{5,15} - 18_{5,14}$	81.3	140.2	5529 (5366, 1.03)	$\leq 1.1 \times 10^{12}$	6×10^{21}	$\leq 2 \times 10^{-10}$	3
L1448R2	[*]102317.1	$19_{3,17} - 18_{3,16}$	60.7	146.9	5529 (5366, 1.03)	$\leq 1.7 \times 10^{12}$	3.5×10^{23}	$\leq 5 \times 10^{-12}$	4
L1527	102979.2	$4_{2,2} - 3_{1,3}$	7.7	8.1	480 (479, 1.00)	$\leq 2.2 \times 10^{11}$	2.8×10^{22}	$\leq 8 \times 10^{-12}$	4
L1544	83332.5	$6_{2,5} - 6_{1,6}$	10.6	13.5	365 (365, 1.00)	$\leq 2.3 \times 10^{11}$	5×10^{21}	$\leq 5 \times 10^{-11}$	5
SVS13A	[*]241325.9	$18_{5,13} - 18_{4,14}$	76.4	39.7	8906 (8262, 1.08)	$\leq 3.9 \times 10^{15}$	3×10^{24}	$\leq 1 \times 10^{-9}$	6
TMC1	150522.0	$3_{3,0} - 2_{2,1}$	13.2	11.1	213 (213, 1.00)	$\leq 3.3 \times 10^{11}$	1×10^{22}	$\leq 3 \times 10^{-11}$	3

Notes. [a]Calculated at the excitation temperature assumed for the source. See Table 3. [b]GBT (PRIMOS) Observations. [c]IRAM 30 m Observations. [*]The spectral line used to calculate the upper limit is a blend of multiple, closely spaced transitions of cyanoketene whose intensities each contribute to the total intensity of the signal. The displayed transitions are representative only – the upper limit was derived using the co-added intensities of all transitions convolved with the appropriate line shape function.
References. [1] Lis & Goldsmith (1990); [2] Crockett et al. (2014); [3] Cernicharo et al. (2018); [4] Jørgensen et al. (2002); [5] Vastel et al. (2014); [6] Chen et al. (2009).

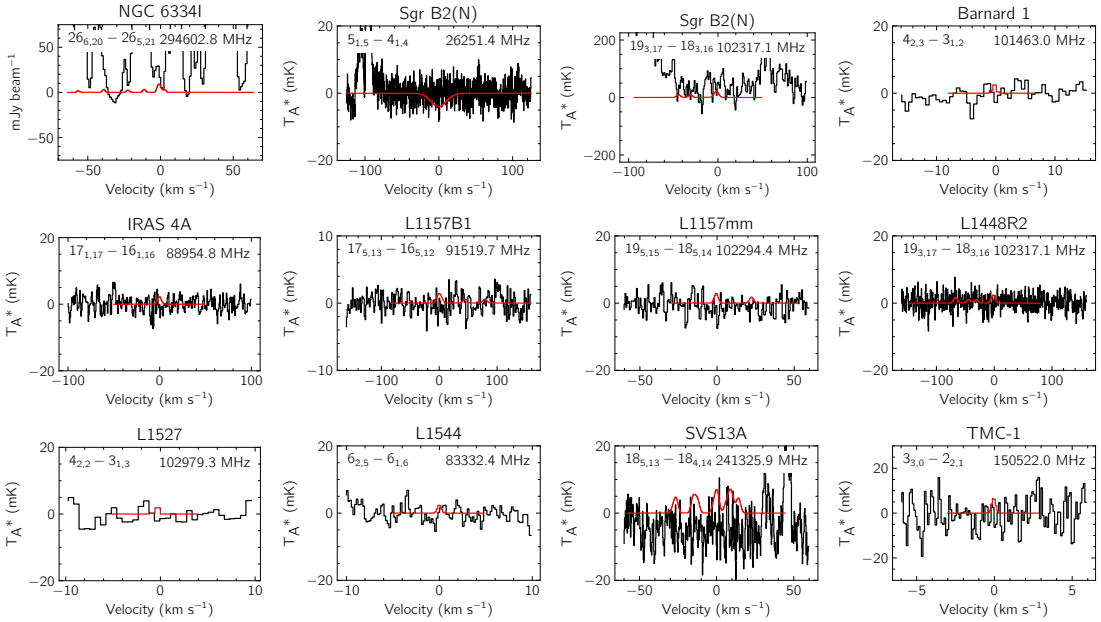

Fig. 2. Transitions of cyanoketene used to calculate the upper limits given in Table 5. In each panel, the red trace shows the transition simulated using the derived upper limit column density and the physical parameters assumed for that source. The frequency of the transition is given in the upper right corner of each panel, and the quantum numbers for each transition in the upper left. The source name is given above each panel. Due to the large variations between observations, the intensity and velocity axes are not uniform across all panels.

Program. These spectra cover a range of source types from cold, dark clouds to Class 0/1 protostars and shocked outflows. Observational details are given in Lefloch et al. (2018).

4.2. Upper-limit analysis and results

We find no definitive evidence for the presence of cyanoketene in any of the sources we have studied. We derive upper limits to the column density in each source using the formalisms outlined in Turner (1991), which assume the molecules are well described by a single excitation temperature and include corrections for optical depth. Frequencies, energy levels, degeneracies, and line strengths were obtained from the laboratory spectroscopy described in this work.

The rotational partition function was obtained and used without modification from SPCAT. In all but the coldest ($T \sim 10$ K) sources, the vibrational contribution to the partition function must also be considered. To that end, we carried out quantum chemical calculations using Gaussian 09 (Frisch et al. 2009) at the wB97XD/6-311++G(d,p) level of theory and basis set to determine the harmonic frequencies of cyanoketene. The structure was first optimized, resulting in equilibrium rotational constants ($A = 30\,101$ MHz, $B = 2814$ MHz, $C = 2573$ MHz) in good agreement with the experimental values. The harmonic frequencies are given in Table 4.

For each source, a simulated spectrum was generated using the physical conditions for the source and the line parameters measured in this work. The 1σ upper limit to the column density

was then derived using the line that gave the most rigorous constraint (i.e.s the line that would have the highest signal-to-noise ratio in the event of a detection). These lines (or a representative transition when multiple transitions contributed to a single spectral feature) and their parameters are provided in Table 5 along with the resulting upper limits. The spectra from each dataset, along with a simulated line profile of cyanoketene at the established upper limit, are displayed in Fig. 2.

From a chemical formation point of view, reactions resulting in addition of a CN group (–CN-addition reactions) involving either neutral or radical species are a viable pathway to the formation of larger cyanides (Bennett et al. 2010; Garrod et al. 2017). Remijan et al. (2008) presumed that a chemical formation route to cyanoformaldehyde (CNCHO) through –CN addition to H_2CO might take place given the high abundances of H_2CO and –CN in the gas phase. Current studies (Das et al. 2013) have followed up this supposition to measure not only the gas-phase and grain-surface reaction rates for this formation pathway but also possible destruction pathways of NCCHO. The results of these analyses showed that NCCHO could be formed efficiently on the grain surfaces, yet a viable desorption mechanism would need to be present to liberate the abundance of NCCHO into the gas phase – such a mechanism could exist in the form of low-velocity shocks. In this work, it is proposed that cyanoketene (NCCHCO) can be formed in similar reaction pathways to cyanoformaldehyde through the following chemical reactions:

1. $H_2CCO + CN \rightarrow NCCHCO + H$ (radical-neutral),
2. $HCCO + CN \rightarrow NCCHCO$ (radical-radical),
3. $C_3N + H_2O \rightarrow NCCHCOH \rightarrow$ followed by H-atom dissociation to form NCCHCO.

In all cases, no experimental or theoretical values exist for the reaction rates of either of the three pathways. Reaction (3), if it is indeed barrier-less (or has a very low barrier), is more likely to form:

1. $C_3N + H_2O \rightarrow HC_3N + OH$ (or $NCCCOH + H$).

As such, additional spectroscopy and astronomical searches are needed for the ethynol radical (HCCOH), a structural isomer of ketene, and its –CN substituted species cyanoethynol (NCCOH). Of the two remaining reactions, (1) would suffer from the same limitations as the formation of NCCHO, and would most likely be most efficiently formed on grain surfaces. Furthermore, while the radical–radical reaction shown in reaction (2) would most certainly occur, the reaction products would also only survive if it occurs on a grain surface. However, unlike the formation and subsequent desorption of NCCHO into the gas-phase, the nondetection of HCNCCO could indicate that: (1) the abundance of NCCHCO on the grain surface is too low to be detectable via current instrumentation when the species is liberated from the grain surface; (2) the desorption mechanisms to liberate the species into the gas phase are either too inefficient or result in the destruction of the molecule; (3) high barriers exist to its formation either in the gas phase or on grain surfaces, and/or (4) effective and efficient gas-phase destruction pathways are present that destroy the molecule quickly after liberation into the gas phase. If this is the case, NCCHCO may only be detectable on grain surfaces, and in any case, further investigation into the formation, destruction, and desorption pathways of NCCHCO is warranted.

The millimeter wave spectra of cyanoketene, a cyano derivative of ketene detected in the ISM, were measured and analyzed. This enabled the accurate prediction of the spectrum up to 400 GHz. It was searched for in major COM sources, but was not detected; upper limits on column density are provided. This work will benefit the astrophysics community for a possible detection in the future.

Acknowledgements. The present investigations were supported by the CNES and the CNRS program "Physique et Chimie du Milieu Interstellaire" (PCMI). This manuscript makes use of the following ALMA data: ADS/JAO.ALMA#2015.A.00022.T and #2017.1.00717.S. ALMA is a partnership of ESO (representing its member states), NSF (USA) and NINS (Japan), together with NRC (Canada) and NSC and ASIAA (Taiwan) and KASI (Republic of Korea), in cooperation with the Republic of Chile. The Joint ALMA Observatory is operated by ESO, AUI/NRAO and NAOJ. The National Radio Astronomy Observatory is a facility of the National Science Foundation operated under cooperative agreement by Associated Universities, Inc. The Green Bank Observatory is a facility of the National Science Foundation operated under cooperative agreement by Associated Universities, Inc. Support for B.A.M. was provided by NASA through Hubble Fellowship grant #HST-HF2-51396 awarded by the Space Telescope Science Institute, which is operated by the Association of Universities for Research in Astronomy, Inc., for NASA, under contract NAS5-26555. J.-C. G. thanks the Centre National d'Etudes Spatiales (CNES) for a Grant.

References

Agúndez, M., Cernicharo, J., & Guélin, M. 2015, A&A, 577, L5
Araki, M., Takano, S., Sakai, N., et al. 2017, ApJ, 847, 1
Belloche, A., Müller, H. S. P., Menten, K. M., Schilke, P., & Comito, C. 2013, A&A, 559, A47
Bennett, C. J., Morales, S. B., Le Picard, S. D., et al. 2010, Phys. Chem. Chem. Phys., 12, 8737
Bermúdez, C., Tercero, B., Motiyenko, R., et al. 2018, A&A, 619, A92
Bock, H., Hirabayashi, T., & Mohmand, S. 1981, Chem. Ber., 114, 2595
Cernicharo, J., Lefloch, B., Agúndez, M., et al. 2018, ApJ, 853, L22
Chen, X., Launhardt, R., & Henning, T. 2009, ApJ, 691, 1729
Chibueze, J. O., Omodaka, T., Handa, T., et al. 2014, ApJ, 784, 114
Crapsi, A., Caselli, P., Walmsley, C. M., et al. 2005, ApJ, 619, 379
Crockett, N. R., Bergin, E. A., Neill, J. L., et al. 2014, ApJ, 787, 112
Das, A., Majumdar, L., Chakrabarti, S. K., Saha, R., & Chakrabarti, S. 2013, MNRAS, 433, 3152
Frisch, M. J., Trucks, G. W., Schlegel, H. B., et al. 2009, Gaussian 09, Revision B.01 (Wallingford, CT: Gaussian, Inc.)
Garrod, R., Belloche, A., Müller, H., & Menten, K. 2017, A&A, 601, A48
Gratier, P., Majumdar, L., Ohishi, M., et al. 2016, ApJS, 225, 1
Guennoun, Z., Piétri, N., Couturier-Tamburelli, I., & Aycard, J.-P. 2004, Chem. Phys., 300, 23
Guennoun, Z., Piétri, N., Couturier-Tamburelli, I., & Aycard, J.-P. 2005, J. Phys. Chem. A, 109, 8299
Hahn, M., Bodenseh, H.-K., & Ferner, M. 2004, J. Mol. Spectrosc., 223, 138
Higuchi, A. E., Sakai, N., Watanabe, Y., et al. 2018, ApJS, 236
Hily-Blant, P., Faure, A., Vastel, C., et al. 2018, MNRAS, 480, 1174
Hollis, J. M., Jewell, P. R., Remijan, A. J., & Lovas, F. J. 2007, ApJ, 660, L125
Jørgensen, J. K., Schöier, F. L., & van Dishoeck, E. F. 2002, A&A, 389, 908
Kisiel, Z. 2001, Spectroscopy from Space (Springer), 91
Lefloch, B., Bachiller, R., Ceccarelli, C., et al. 2018, MNRAS, 477, 4792
Lis, D. C., & Goldsmith, P. F. 1990, ApJ, 356, 195
Maier, G., Reisenauer, H. P., & Rademacher, K. 1998, Chem. Eur. J., 4, 1957
McGuire, B. A. 2018, ApJS, 239, 17
McGuire, B. A., Carroll, P. B., Dollhopf, N. M., et al. 2015, ApJ, 812, 1
McGuire, B. A., Carroll, P. B., Loomis, R. A., et al. 2016, Science, 352, 1449
McGuire, B. A., Shingledecker, C. N., Willis, E. R., et al. 2017, ApJ, 851, L46
McGuire, B. A., Brogan, C. L., Hunter, T. R., et al. 2018a, ApJ, 863, L35
McGuire, B. A., Burkhardt, A. M., Kalenskii, S. V., et al. 2018b, Science, 359, 202
Melosso, M., Melli, A., Puzzarini, C., et al. 2018, A&A, 609, A121
Neill, J. L., Muckle, M. T., Zaleski, D. P., et al. 2012, ApJ, 755, 153
Pickett, H. M. 1991, J. Mol. Spectrosc., 148, 371
Reid, M. J., Menten, K. M., Brunthaler, A., et al. 2014, ApJ, 783, 130
Remijan, A. J., Hollis, J. M., Lovas, F. J., et al. 2008, ApJ, 675, L85
Snyder, L. E., Buhl, D., Zuckerman, B., & Palmer, P. 1969, Phys. Rev. Lett., 22, 679
Turner, B. 1977, ApJ, 213, L75
Turner, B. E. 1991, ApJS, 76, 617
Vastel, C., Ceccarelli, C., Lefloch, B., & Bachiller, R. 2014, ApJ, 795, L2
Zakharenko, O., Motiyenko, R. A., Margulès, L., & Huet, T. R. 2015, J. Mol. Spectrosc., 317, 41